

Article

Peptide-Functionalized Nanoparticles for the Targeted Delivery of Cytotoxins to MMP-14-Expressing Cancer Cells

Jillian Cathcart^{1,2}, Giulia Suarato³ , Weiyi Li³, Jian Cao¹ and Yizhi Meng^{3,*}¹ Department of Medicine, State University of New York, Stony Brook, NY 11794, USA² Department of Molecular and Cellular Pharmacology, State University of New York, Stony Brook, NY 11794, USA³ Department of Materials Science and Chemical Engineering, State University of New York, Stony Brook, NY 11794, USA

* Correspondence: yizhi.meng@stonybrook.edu; Tel.: +1-(631)-632-8552

Abstract: As 90% of cancer-patient deaths are due to metastasis, novel therapeutics that selectively target and kill metastatic cells are desperately needed. Matrix metalloproteinase-14 (MMP-14), which plays a critical role in digesting the basement membrane and in inducing cancer cell migration, has been found to be expressed at the cell surface of circulating and metastasized tumor cells in various human cancers. We have recently shown that the IVS4 peptide, which mimics the minimal binding motif of the hemopexin-like (PEX) domain of MMP-14, interrupts MMP-14 dimerization and decreases MMP-14-mediated cell invasion. In this study, cancer-homing nanocarriers were assembled by linking IVS4 to polysaccharide-based nanoparticles (NPs), followed by the encapsulation of a pharmaceutical agent. IVS4-NPs efficiently prevented MMP-14-mediated cell migration and conferred an uptake advantage compared to the control peptide in an MMP-14-dependent manner. While the IVS4-NPs alone were not cytotoxic, drug-encapsulated NPs were shown to effectively target MMP-14-expressing cancer cells. This novel nanotherapeutic is capable of inhibiting MMP-14-mediated functions and efficiently killing MMP-14-expressing cancer cells, without affecting the viability of non-cancer cells.

Keywords: metastasis; breast cancer; MMP-14; chitosan nanoparticles

Citation: Cathcart, J.; Suarato, G.; Li, W.; Cao, J.; Meng, Y. Peptide-Functionalized Nanoparticles for the Targeted Delivery of Cytotoxins to MMP-14-Expressing Cancer Cells. *Biophysica* **2022**, *2*, 203–220. <https://doi.org/10.3390/biophysica2030021>

Academic Editors: Ricardo L. Mancera, Paul C Whitford and Chandra Kothapalli

Received: 6 August 2022

Accepted: 22 August 2022

Published: 24 August 2022

Publisher's Note: MDPI stays neutral with regard to jurisdictional claims in published maps and institutional affiliations.



Copyright: © 2022 by the authors. Licensee MDPI, Basel, Switzerland. This article is an open access article distributed under the terms and conditions of the Creative Commons Attribution (CC BY) license (<https://creativecommons.org/licenses/by/4.0/>).

1. Introduction

Despite overwhelming advances in our understanding of cancer progression, current therapeutics still fall short of targeting the deadliest aspect: metastasis. Accounting for 90% of cancer-patient deaths [1], metastasis is a multi-step coordinated process that renders cells the ability to degrade the basement membrane and surrounding extracellular matrix (ECM), intravasate into blood or lymph, and extravasate to set up a secondary colony. Membrane-type matrix metalloproteinase 14 (MMP-14, known as MT1-MMP) is an endo-protease commonly expressed in cancer and is associated with increased cell migration and invasion [2,3], angiogenesis [4,5], metastasis [6,7], and poor patient prognosis [2,8]. MMP-14 activity relies on its expression at the cell membrane and can be regulated at the transcriptional level as well as where the protease is localized. The internalization of MMP-14 proceeds via receptor-mediated endocytosis upon the binding of substrates or as part of normal cellular functions.

Previous research into MMP inhibitors (MMPIs) has been unsuccessful, as clinically tested MMPIs targeted the catalytic domain and chelated the catalytic zinc ion responsible for facilitating catalysis. In hindsight, this was a poor strategy, as the catalytic domain is highly conserved among the two dozen MMP family members and is extremely like the catalytic domain found in a disintegrin and metalloproteinase (ADAM) family members. To increase selectivity for MMP-14, we sought to target the hemopexin-like domain (PEX) of MMP-14, a domain responsible for facilitating substrate recognition and the dimerization

required to confer metastatic abilities to cancer cells. Importantly, there is considerably less homology between the hemopexin-like domains within the metalloproteinase family members [9–11]. The PEX domain of MMP-14 is a four-bladed propeller-like structure, with each blade consisting of four strands, and homodimerization of MMP-14 is found to occur via interactions of the fourth strand of the fourth blade in each molecule. Recently, our group designed a long peptide (termed IVS4), eight amino acid residues in length, which disrupts this dimerization, thus attenuating MMP-14-mediated functions such as invasion and cell migration [2]. As peptides are rapidly cleared from circulation and have poor tissue distribution, we developed a novel bifunctional drug delivery system by incorporating the IVS4 peptide into polymeric nanoparticles (NPs). We hypothesized that the route of endocytosis of MMP-14 can aid in the selective targeting of functionalized, drug-loaded NPs against metastatic cancer. In this study, we bioconjugated the IVS4 peptides to hydrophobically modified glycol chitosan NPs and demonstrated their ability to bind to MMP-14 and inhibit MMP-14-mediated functions *in vitro* and *in vivo*. Moreover, the binding of IVS4 to MMP-14 expressed at the cell surface facilitated receptor-mediated endocytosis of the NPs into cancer cells. Encapsulation of cytotoxin ansamitocin P-3, a potent microtubule destabilizer [12–14], by the NPs allowed for a selective release of the active drug into cancer cells, while leaving normal, healthy cells viable. Our NP-encapsulation system may serve as a prototypical model for developing strategies to minimize the off-target effects of highly toxic cancer drugs.

2. Materials and Methods

2.1. Materials

Biotinylated peptides (IVS4 peptide Biotin-GYPKSALR-NH₂, 1116.37 Da and generic control peptide Biotin-GIHTEIGK-NH₂, 1079.31 Da) were customarily synthesized by EZBiolab (Carmel, IN, USA). Glycol chitosan (250 kDa molecular weight, degree of deacetylation > 60%), 5 β -cholanolic acid, N-(3-dimethylaminopropyl)-N'-ethylcarbodiimide hydrochloride (EDC), N-hydroxysuccinimide (NHS), and HPLC-grade (>90% purity) ansamitocin P-3 (AP3) were purchased from Sigma-Aldrich (St. Louis, MO, USA). Monoreactive hydroxysuccinimide ester of Cyanine 3 (Cy3-NHS) was obtained from Lumiprobe (Cockeysville, MD, USA). Anti-MMP-14 antibody against the hemopexin domain was purchased from EMD Millipore (Burlington, MA, USA). Horseradish peroxidase (HRP)-conjugated anti-mouse and anti-rabbit secondary antibodies were acquired from Rockland Immunochemicals (Pottstown, PA, USA). Anti-actin antibody was obtained from Cell Signaling Technologies (Danvers, MA, USA). Anti-MMP-14 antibody against the Hinge region (Ab6004, used for IF) was purchased from Millipore (Burlington, MA, USA). Anti-EEA-1 (clone 14) was purchased from BD Biosciences (Franklin Lakes, NJ, USA). Anti-LAMP-1 (ab24170) and anti-Giantin (clone 9B6) were purchased from Abcam (Cambridge, UK). Fluorescent secondary antibodies were purchased from Molecular Probes (Eugene, OR, USA). Dynamin2-k44a plasmid (K44A HA-dynamin 2 pcDNA3.1 plasmid 34683) and the far-red plasmid used as a positive control for transfection (pcDNA3-mNeptune2.5 plasmid 51310) were purchased from Addgene (Watertown, MA, USA).

2.2. MMP-14 PEX Protein Purification

The MMP-14 hemopexin-like domain (PEX) was cloned into vector pet16b using a PCR approach from HT-1080 cells using forward primer 5'-GATCATATGGGGCCCAACATCTGT GACGGGAA-3' and reverse primer 5'-GATCTCGAGTCATCCCCGATGGGCAGCCCATCCA-3'. Restriction enzymes Nde I and Xho I were used. Chemically competent *E. coli* BL21 Arctic Express (DE3) cells were transformed with pET-16b-MMP-14-PEX. A single colony was chosen for amplification in LB medium in the presence of 100 μ g/mL ampicillin and grown at 37 °C, with shaking to an OD₆₀₀ of 0.5–0.8. The temperature was then decreased to 15 °C, and MMP-14-PEX synthesis was induced with 250 μ M isopropyl β -D-1-thiogalactopyranoside (IPTG). After 4 h, cells were harvested by centrifugation at 4000 RPM for 20 min at 4 °C. The pellet then went through two freeze–thaw cycles and

was resuspended in lysis buffer (50 mM Tris-Cl, 100 mM NaCl, 10 mM EDTA, 2% Triton, 100 μ M phenylmethylsulfonyl fluoride (PMSF), 500 μ g/mL DNase, pH 8.0) and incubated for 2 h at 4 °C with gentle agitation. The lysate was then sonicated and centrifuged at 4 °C at 15,000 \times *g* for 15 min. The soluble fraction (supernatant) was then collected and MMP-14-PEX protein was purified using Ni-NTA agarose resin (Qiagen, Hilden, Germany) using the Amicon Centrifugal Filter Units (Millipore, Burlington, MA, USA), in accordance with the instructions of the manufacturer. Prior to elution, the protein was washed with wash buffer (50 mM NaH₂PO₄, 300 mM NaCl, 20 mM imidazole, pH 8.0) and then eluted with elution buffer (50 mM NaH₂PO₄, 300 mM NaCl, 250 mM imidazole, pH 8.0). Eluate was then dialyzed against (50 mM NaH₂PO₄, 300 mM NaCl, 5% glycerol *v/v*, pH 8.0). Protein purity was assessed by SDS-PAGE. Monomeric units of MMP-14-PEX were then isolated by size exclusion chromatography on a HiLoad 16/60 Superdex 200 column (GE Healthcare, Chicago, IL, USA) in elution buffer. The concentration of the combined fractions containing monomers only was analyzed using Beer's Law. Protein was concentrated using the Amicon Centrifugal Filter Device (Millipore, Burlington, MA, USA). Concentrated protein was then aliquoted and stored at –80 °C. Folding of the purified protein was evaluated by two thermal denaturation assays via analysis of intrinsic protein fluorescence and monitoring of fluorescence of the reporter dye Sypro Orange, as has been described previously [15].

2.3. Preparation of Ansamitocin P-3 Encapsulated Cy3-HGC Nanoparticles

To introduce the IVS4 or control peptides, glycol chitosan was biotinylated. Firstly, 17 mg sulfo-NHS-LC-Biotin dissolved in 2 mL HPLC water was added dropwise and allowed to react for 3 h with stirring. The solution was then loaded into cassettes and dialyzed for 48 h (10 kDa MWCO, ThermoScientific, Waltham, MA, USA). After 3 days of lyophilization, biotinylated glycol chitosan powder was obtained. Then, 300 mg of the resulting material were further re-suspended in 50 mL HPLC water, and avidin (80 mg in 10 mL HPLC water) was added dropwise. After 2 h of stirring, the solution was transferred to Amicon tubes (100 kDa MWCO, ThermoScientific, Waltham, MA, USA) and centrifuged for 30 min at 5000 \times *g*. The resulting retentate was freeze-dried and ground into powder to obtain avidinated biotinylated glycol chitosan. Next, the product was hydrophobically modified with 5 β -cholanic acid (Figure 1B), dialyzed to remove unreacted material, and lyophilized to produce avidinated biotinylated hydrophobically modified glycol chitosan (HGC). In the last step of the reaction process, 77 μ L of the biotinylated peptides suspended in DMSO were added dropwise and allowed to react for 2 h at room temperature in the dark, with gentle stirring. At this point, the Cy3 fluorophore was also introduced in the reaction mixture, as previously described. Following dialysis, freeze-drying, and grinding, peptide-Cy3-HGC complex was obtained as resulting product.

To load ansamitocin P-3 (AP3) into the HGC nanoparticles, 30 mg of IVS4-Cy3-HGC was suspended in 9 mL DMSO for 1 h in the dark at room temperature, under gentle stirring. Subsequently, 1.55 mg AP3 dissolved in 0.776 mL DMSO was added dropwise. The reagents were allowed to mix for 5 h, before 21 mL of HPLC water were added, to facilitate the formation of micelles [16]. After an overnight incubation in the dark at room temperature, under gentle stirring, dialysis was performed using dialysis cassettes (3.5 kDa MWCO, ThermoScientific, Waltham, MA, USA) against HPLC water for 48 h, to remove non-encapsulated drug molecules. The purified system was then centrifuged for 30 min at 5000 \times *g*, lyophilized for 3 days, and then ground into a fine powder to obtain the AP3-loaded IVS4-Cy3-HGC complex (AP3-IVS4-Cy3-HGC).

Prior to use, the nanoparticle powder was suspended in serum-free sterile media at the desired stock concentration (typically 500 μ g/mL) and vortexed. The suspension was then sonicated for 6 min with a probe-type sonifier (Soniprep 150, MSE, UK), equipped with an exponential probe under an ice bath to prevent any increase in the temperature. The self-assembled nanoparticles were then passed through syringe filters (pore sizes 0.8 and

0.2 μm , Pall Corporation, Port Washington, NY, USA) in order to sterilize the suspension, prior to characterization and cell culture delivery.

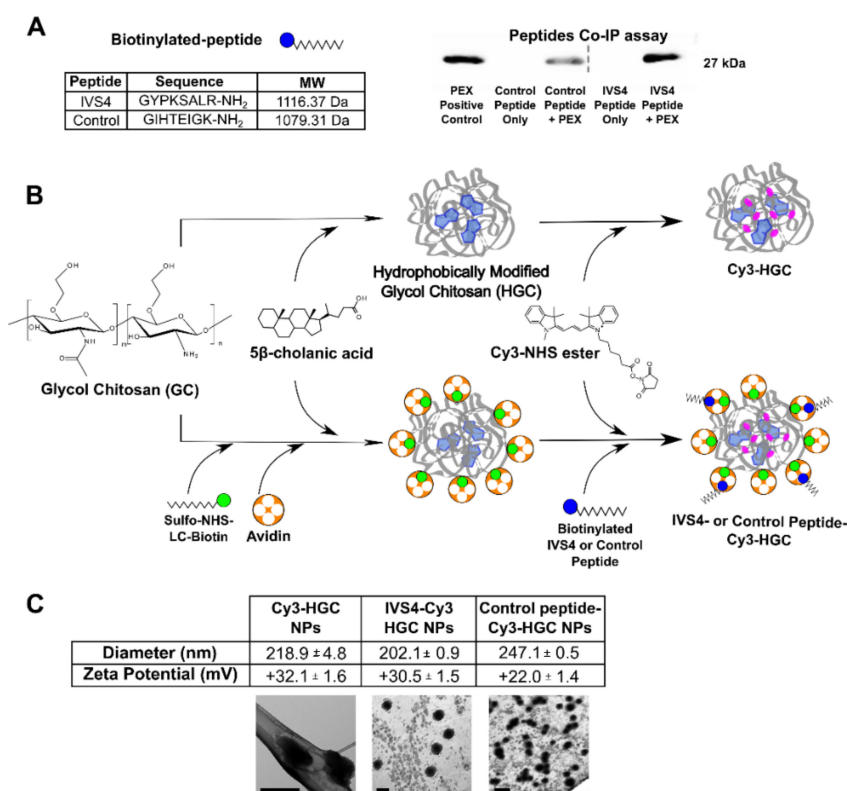


Figure 1. IVS4 peptide is specific for the MMP-14 hemopexin domain: (A) A modified pull-down using the biotinylated IVS4 peptide or control bound to streptavidin beads after incubation with or without purified MMP-14-hemopexin-like domain (PEX) demonstrates that IVS4 peptide binds significantly more PEX than control peptide. Dashed line indicates where another tested condition not discussed herein has been cropped out. Synthesis of peptide-functionalized nanoparticles: (B) Glycol chitosan is first coupled with biotin, followed by binding with avidin. Hydrophobic modification is performed via reaction with 5 β -cholanic acid to yield a micellar nanoparticle. Biotinylated peptides (IVS4 and control peptides) are incorporated into the nanoparticle via the biotin-avidin binding, and Cy3 fluorophore is conjugated to the backbone of glycol chitosan. As control, a similar synthesis protocol is performed to obtain plain, non-peptide-functionalized nanoparticles. Physico-chemical and morphological features of the synthesized nanocomplexes: (C) TEM images confirmed the formation of spheroid-like nanoparticles. Dynamic light scattering and zeta potential analyses revealed homogenous sizes and positively charged surfaces. Scale bars, 500 nm.

2.4. Physicochemical Characterization of Nanoparticles

The size distribution and surface charge of the HGC nanoparticles were determined at 25 °C by Dynamic Light Scattering (DLS, Zetasizer Nano, Malvern Instruments Ltd., Westborough, MA, USA). The morphology was obtained by placing a few drops of HGC nanoparticle suspension on Lacey Carbon Film on 300 mesh copper grids, and the extra solution was blotted with filter paper and air dried. The grids were observed under a transmission electron microscope (JEM-1400LaB6, JEOL, Japan) with an accelerating voltage of 60 kV.

2.5. Cell Culture and Transfection

All cell lines used in this study, except TMD-231-LM2, were purchased from the American Type Culture Collection (ATCC, Manassas, VA, USA) and cultured as recommended. The TMD-231-LM2 cell line was kindly provided to us by Dr. Joan Massague (Memorial

Sloan Kettering Cancer Center, New York, NY, USA). The MDA-MB-231 and TMD-231-LM2 cells were cultured in DMEM containing 10% FBS under 5% CO₂. The MCF-10A cells were cultured in a 50/50 mixture of DMEM/F-12 with 5% horse serum, 20 ng/mL epidermal growth factor (EGF), 0.5 mg/mL hydrocortisone, 100 ng/mL cholera toxin, and 10 µg/mL insulin. The SK-3rd cells were cultured in ultra-low attachment culture dishes in suspension with serum-free DMEM-F12 supplemented with B27 (1:50), 20 ng/mL EGF, 0.4% bovine serum albumin, and 4 mg/mL insulin. Hypoxia experiments were performed at 5% CO₂, 1% O₂, and 37 °C in a ProOx C21 Hypoxia chamber (Biospherix, Parish, NY, USA). To achieve transient transfection of cells, TurboFect was incubated with plasmid DNA for 30 min at room temperature prior to addition to cells, in accordance with the protocol of the manufacturer. Medium was replaced after 18 h, and assays were performed after the indicated recovery period. Cos-1-MMP-14 and Cos-1-pQXCIP (Cos-1-pQ) stable cells were generated, as previously described [2,17]. Briefly, the MT1-MMP cDNA encoding an open reading frame from amino acid residues Met¹-Val⁵⁸² was produced via PCR with forward primer (5' to 3', CACGAATTCCGGACCATGTCTCCCGCCCAAGA) and reverse primer (5' to 3', AAGGATCCCCTTCGAACATTGGCCTTGA). The PCR fragments were digested by XhoI and BglII, and the resultant fragments were then cloned into the pQXCIP retroviral vector at XhoI and BamHI sites. The resulting plasmid was co-transfected into human embryonic kidney GP2-293 packaging cells (Clontech, Japan), in accordance with the protocol of the manufacturer. Cos-1 cells were subsequently infected with the supernatant containing the retrovirus in the presence of polybrene and selected with puromycin.

2.6. Dot-Based Cell Migration Assay

Migration assays were performed, as previously described [18]. Briefly, MDA-231 cells were pre-treated for thirty minutes with the indicated treatment, embedded into a collagen matrix (final concentration 1.5 mg/mL rat tail type I collagen, 1× DMEM, 50% cell pellet, pH 7.5), and dotted in a 96-well plate. Solidified cell-matrix dots were overlaid with 2.5 µg/mL of the indicated treatment or vehicle control suspended in complete media DMEM. Cells were allowed to migrate for up to 8 h, fixed in paraformaldehyde at a final concentration of 4%, and then stained in Hoechst/PBS (1:2000). Microscopy images were captured at 10× using a Nikon microscope and camera system, and migration was quantified by counting nuclei using the Nikon Elements Basic Research Software analysis tools.

2.7. MMP-14 Association and Endocytosis Mechanism Studies

Triple-negative breast cancer MDA-MB-231 cells were plated on glass-bottom coverslips. The following day, cells were transferred at 4 °C for 15 min to pre-adapt and then were treated, on ice, with 2.5 µg/mL IVS4-Cy3-HGC nanoparticles and anti-MMP-14 antibody in serum-free DMEM. Samples were incubated at 4 °C for 1 h to halt endocytosis, while the IVS4 moiety on the nanoparticles interacted with the PEX domain of cell-surface MMP-14. Subsequently, cells were washed with ice cold PBS to remove the unbound nanoparticles and then transferred at 37 °C to initiate endocytosis for different time points (0, 2, 5, 10, 30 min). Cells were fixed with 4% paraformaldehyde for 20 min at room temperature and then permeabilized with Triton 0.02% for 7 min. After PBS washings, samples were blocked with 1% BSA and 5% normal goat serum for 30 min and then treated with fluorescent secondary antibody for 1 h. Afterwards, nuclei were stained with Hoechst. Samples were imaged with a Nikon N-SIM Super Resolution Microscope equipped with a red laser (543 nm), a green laser (488 nm), and a blue laser (405 nm).

Intracellular trafficking of the nanoparticles was examined in MDA-MB-231 cells using immunofluorescence microscopy. Cells were plated and treated as described in the MMP-14 associated mechanism study but without the primary anti-MMP-14 antibody. MDA-MB-231 cells were incubated at 4 °C prior to being transferred to the 37 °C incubator at pre-determined time points. Cells were then fixed at 30 min, 1 h, 3 h, 8 h, 18 h, and 24 h, blocked as above, and stained with either primary antibody for early endosomes (EEA1), lysosomes (LAMP1), or trans-Golgi network (giantin). Appropriate fluorescent secondary

antibodies were used, and cells were Hoechst-stained. Control samples, in which cells were not treated with Cy3-HGC-IVS4 nanoparticles, were also considered for time points 0 and 24 h, as comparison. Samples were imaged with a Nikon N-SIM Super-resolution Structured Illumination Microscope (SIM) equipped with a red laser (543 nm), a green laser (488 nm), and a blue laser (405 nm). Nanoparticles were determined to be uptaken by a cell when their fluorescence signal (visualized in the red channel) co-localized within the perinuclear space.

2.8. Encapsulation Efficiency and Loading Capacity

To calculate the encapsulation efficiency and loading capacity, the absorbance of NPs at 250 nm was determined using a spectrophotometric plate reader (Tecan Infinite 200 PRO, Tecan Austria GmbH, Grödig, Austria). The total mass of encapsulated AP3 was extrapolated using a standard curve. Encapsulation efficiency was calculated as the mass of AP3 entrapped in the NPs divided by the mass of AP3 in the feedstock. Loading capacity was calculated as the mass of AP3 entrapped in the NPs divided by the mass of the NPs in the feedstock.

2.9. Release Kinetics

Release behavior of AP3 from IVS4-Cy3-HGC NPs was evaluated at pH 7.4 and pH 5.5 using UV-vis spectrophotometry. Briefly, freeze-dried ansamitocin P3-loaded IVS4-Cy3-HGC powder was suspended in phosphate-buffered saline (PBS, pH 7.4). The system was kept under gentle shaking at room temperature in the dark. At predetermined time intervals, samples were taken for evaluation, and the volume was replaced with fresh buffer to maintain the sink conditions. To compare the effect of pH on release behavior, this experiment was performed in parallel at pH 5.5. For the detection of the released AP3, a UV-vis spectroscopic plate reader was used (Tecan Infinite 200 PRO, Tecan Austria GmbH, Grödig, Austria), and absorbance was measured at 250 nm. The amount of AP3 released was calculated using a standard curve.

2.10. Chicken Chorioallantoic Membrane (CAM) Assay

Fertilized white chicken eggs (SPF Premium, Charles River Laboratory, CT) were incubated at 37 °C in 70% humidity for 10 days. At that time, the CAM was dropped to facilitate the drilling of a small window into the egg, as previously reported in the literature [19]. A total of 10⁶ TMD-231-LM2 cells were pre-treated with the indicated condition for 30 min at room temperature and then embedded in a collagen/media matrix (3 mg/mL), before delivery onto the CAM surface. Each egg was exposed to AP3-loaded IVS4-Cy3-HGC NPs, IVS4-Cy3-HGC NPs, control peptide-Cy3-HGC NPs, or the NP vehicle. Over the course of the next seven days, the CAMs were treated as indicated three times. The dropped and treated CAM tissue in the window region of the egg was then dissected, formalin-fixed, and embedded in optimal cutting temperature (OCT) compound. CAMs were cryosectioned 8 µm thick and stained with hematoxylin and eosin (H&E). Analyses were performed with the help of Jingxuan Liu, Department of Pathology, Stony Brook University, Stony Brook, NY, USA.

2.11. Statistical Analysis

All experiments were performed a minimum of three times unless otherwise noted. Statistical analyses using the indicated tests were performed using GraphPad. Graphical analyses are results of a representative experiment, unless otherwise noted.

3. Results

3.1. Development of MMP-14 Homing Peptide–Nanoparticle Delivery System

Previously, we demonstrated that peptides specific for the hemopexin domain of MMP-14 were capable of disrupting MMP-14-mediated functions [2]. To further confirm if the disruption of functional MMP-14 is due to the physical interaction between the MMP-14

specific peptide (named IVS4) and the MMP-14 hemopexin domain, a modified pulldown assay was performed. We observed a negligible amount of PEX protein after pulldown with the control peptide; however, a substantial amount of hemopexin-like protein was detected by the IVS4 peptides (Figure 1A). This demonstrates that IVS4 indeed binds specifically to the hemopexin-like domain of MMP-14.

Since MMP-14 is expressed at the invasive cancer cell surface, we proceeded to develop an MMP-14-binding peptide-guided cytotoxin, to selectively target invasive cancer cells with a minimal effect on the health of normal cells. In order to tether IVS4 to a polymeric nanoparticle that would help minimize proteolytic degradation, we bioconjugated the peptide to chitosan-based micellar nanoparticles (NPs) via an avidin–biotin binding strategy developed by our group [20,21]. In this approach, a linear polymer, glycol chitosan (GC), was covalently linked to the biotin prior to hydrophobic modification and self-assembly into a micellar nanoparticle (Figure 1B). Biotinylated IVS4 peptide was then non-covalently linked to the nanoparticle via the avidin. The strong avidin–biotin binding helps to stabilize IVS4 and preserve its function. A generic peptide with no known biologic function was used as the control. A cyanine fluorophore (Cy3) was incorporated to facilitate NP visualization (Figure 1B). Particle-size analysis showed that the average NP diameter was between 200 nm and 250 nm (Figure 1C), similar to previous reports [20,22–24]. Analysis of the zeta potential (Figure 1C) showed that the NPs had a positive surface charge (ranging from +22 mV to +32 mV), as expected, due to the polycationic nature of glycol chitosan. Transmission electron microscopy (TEM) demonstrated that the NPs were uniform and spheroid-like (Figure 1C).

3.2. IVS4 Peptide Confers Selectivity to MMP-14-Expressing Cells

To characterize the selectivity of the assembled NPs, an uptake study was performed using Cos-1 monkey fibroblast-like cells stably transfected with MMP-14 cDNA or vector control. After incubation with IVS4-Cy3-HGC NPs, which contain the MMP-14-selective peptide, Cos-1-MMP-14-expressing cells demonstrated a three-fold increase in uptake compared to the Cos-1-pQ vector control cells (Figure 2A,B). Cos-1 cells overexpressing either plasmid demonstrated only minimal uptake of either the Cy3- HGC-NPs or the control peptide-Cy3-HGC NPs, indicating the ability of the IVS4 peptide to confer selectivity for MMP-14-expressing cells. To further support this, an uptake study was also performed on cells endogenously expressing MMP-14 (triple-negative breast cancer cell line MDA-MB-231) and cells lacking endogenous MMP-14 (non-cancerous human breast epithelial MCF-10A cells). While uptake of either Cy3-HGC or control peptide-Cy3-HGC NPs by the MDA-MB-231 triple-negative breast cancer cells was also minimal, as expected, the IVS4-Cy3-HGC NPs were taken up extensively (Figure 2C,D). Specifically, uptake in MDA-MB-231 cells increased nearly three-fold compared to that in MCF-10 cells. The non-MMP-14-expressing control MCF-10A cells took up little or no NPs of any type. To determine if the conjugated MMP-14 peptide, IVS4, can interact with MMP-14 at the cell surface and maintain its inhibitory effect on MMP-14 mediated cell migration, a collagen matrix cell migration assay was performed in the MDA-MB-231 cells. In this study, MDA-MB-231 cells embedded in a collagen matrix were exposed to media containing control peptide-Cy3-HGC or IVS4-Cy3-HGC NPs and incubated for 8 h. Cell number analysis in the “invasion zone” indicated that only IVS4-Cy3-HGC NPs significantly attenuated migration (Figure 2E,F), suggesting that peptide linking to the HGC-NPs does not interfere with the inhibitory function of the MMP-14 peptides.

To evaluate the cytocompatibility of the NPs, a cell viability assay was performed using both MDA-MB-231 breast cancer cells and MCF-10A control cells. No effect on cell viability was observed by any of the three types of NPs for concentrations up to 50 µg/mL (Supplementary Figure S1), indicating that our NP system alone does not induce cell death.

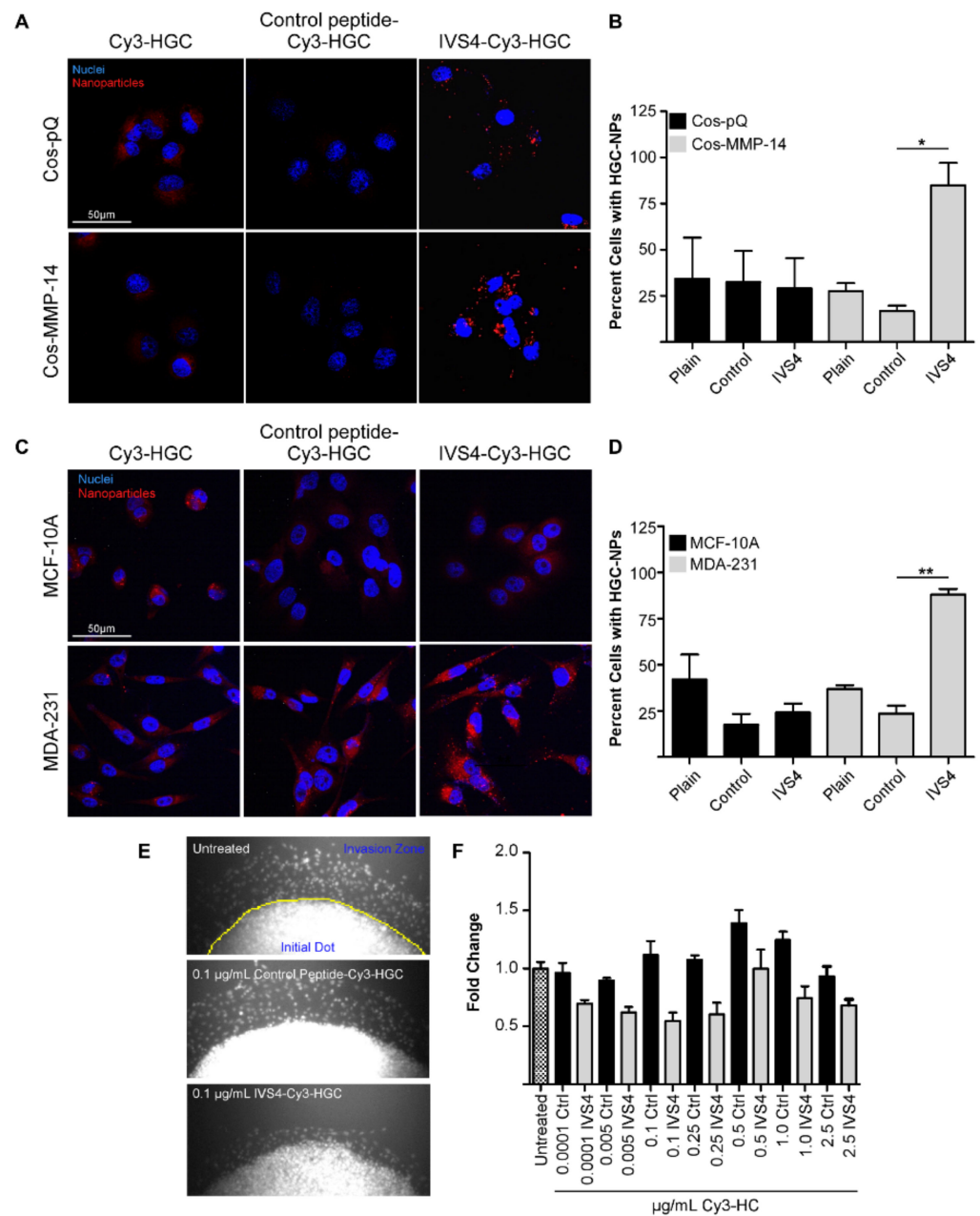


Figure 2. IVS4 peptide confers an uptake advantage to MMP-14-expressing cells. **(A,B)** Delivery of 1.0 µg/mL NPs for 8 h to normal Cos-1 cells that only express vector control: little to no NPs of any type were internalized. In Cos-1 cells stably expressing MMP-14, however, the nanoparticles bearing the IVS4 peptide were internalized more efficiently (* $p < 0.05$ by one-way ANOVA, counts performed on five images per condition). **(C,D)** While no differences are observed in uptake of 2.5 µg/mL Cy3-HGC or control peptide-Cy3-HGC NPs for any cell type, the IVS4-Cy3-HGC NPs were taken up more efficiently after 24 h only in MDA-MB-231 cells (** $p < 0.001$ by one-way ANOVA, counts performed on five images per condition). **(E,F)** The IVS4 peptide-conjugated NPs can significantly attenuate migration of MDA-MB-231 cells ($p < 0.01$ by two-way ANOVA). These experiments were performed in triplicate with combined data represented.

3.3. IVS4-Cy3-HGC NPs Bind to MMP-14 and Are Internalized via Endocytosis

As MMP-14 is known to be internalized by endocytosis, the IVS4 peptide was hypothesized to facilitate targeted delivery of our NPs in an MMP-14-dependent manner. Super-resolution Structured Illumination Microscopy (SIM) was used to visualize endocytic transport. A co-localization study (see Supplementary Figure S2) between MMP-14 and

NPs, based on Cy3 fluorescence intensity, was performed using anti-MMP-14 antibody in MDA-MB-231 cells. After incubation for 1 h at 4 °C (T0) to block endocytosis, the IVS4-Cy3-HGC NPs were observed to co-localize strongly with MMP-14 at the cell surface, as evidenced by a punctate, intense fluorescence signal (Figure 3A). This strongly indicates that the MMP-14 molecules were clustering around the NPs. In addition, the complexes formed by the association of MMP-14 and IVS4-Cy3-HGC NPs appeared to be on the extra-cellular face of the plasma membrane. After transfer to 37 °C and a subsequent 10-minute incubation to re-initiate endocytosis (T10), more MMP-14/IVS4-Cy3-HGC complexes were observed in the intracellular space (Figure 3B). By 30 min (T30), co-localization was still visible in most cells; however, both MMP-14 and IVS4-Cy3-HGC NPs were now found predominantly in the perinuclear regions (Figure 3C).

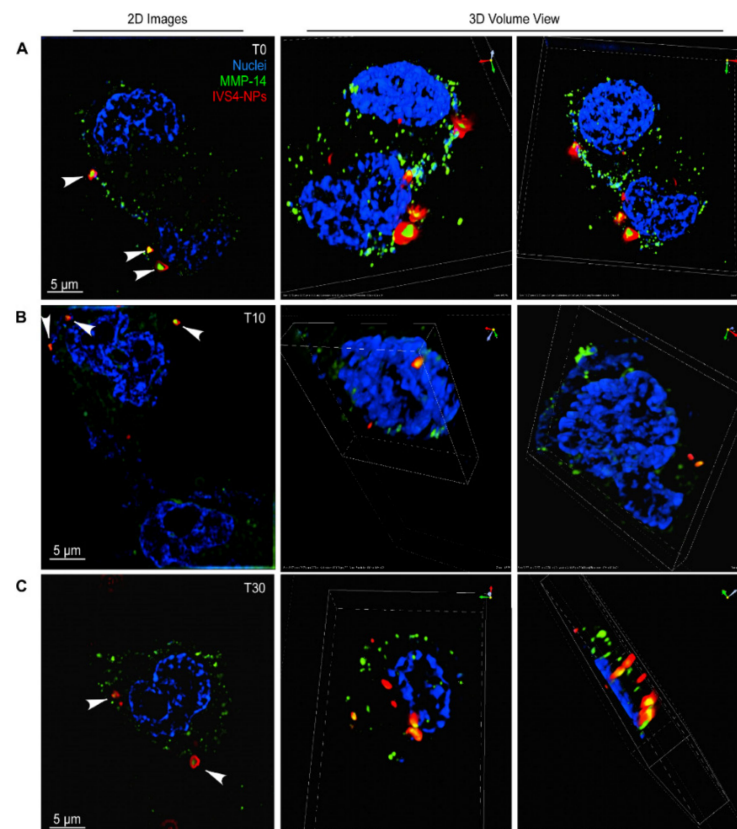


Figure 3. Time-course analysis of IVS4-Cy3-HGC NPs and MMP-14 internalization. (A) After an hour at 4 °C, IVS4-Cy3-HGC NPs (red channel) were found to co-localize with MMP-14 (green channel) at the cell surface of MDA-MB-231 cells (T0). (B) At T10 min, the NPs and MMP-14 remained co-localized but now appeared to be inside the cell. (C) By T30 min, some co-localization was still observed, and the NPs were clearly intracellular and appeared to be perinuclear. Figures on the left-most panel are 2D images, while the right two panels are different 3D views. Arrows indicate areas of MMP-14 and IVS4-Cy3-HGC NP co-localization.

Since endocytic routing can influence nanoparticle disassembly and, ultimately, drug release [25], we next examined the intracellular trajectory of the IVS4-Cy3-HGC NPs in MDA-MB-231 cells. An endocytosis assay was performed, in which cells were incubated at 4 °C prior to being transferred to the 37 °C incubator at pre-determined time points. Cells were then fixed and stained for markers of the different endocytic compartments. After 8 h at 37 °C, endocytosis of the IVS4-Cy3-HGC NPs was confirmed by immunofluorescence for the early endosomal antigen (EEA-1). SIM analysis clearly indicates that the IVS4-Cy3-HGC NPs were trapped within early endosomes (Figure 4A). Interestingly, the overall endosome structure changed drastically over the course of this experiment

(Supplementary Figure S3). Specifically, at time 0, when endocytosis had been halted for the preceding hour by incubation at 4 °C, the endosomes appeared small and punctate, and NP entrapment was not observed, as evidenced by Cy3 fluorescence. Subsequently, the endosomes increased in size, with some NPs entrapped as early as 3 h. At the peak of NP entrapment (8 h), the endosomes appeared to have swollen substantially compared to those at T0. By 18 h, NPs were no longer located inside the endosomes, which now appeared to have regressed in size. A 2011 study by Bacac et al. established this phenomenon to be a characteristic of defective endosomal acidification [26], which may occur as a result of the “proton sponge” effect, following the endocytosis of the NPs.

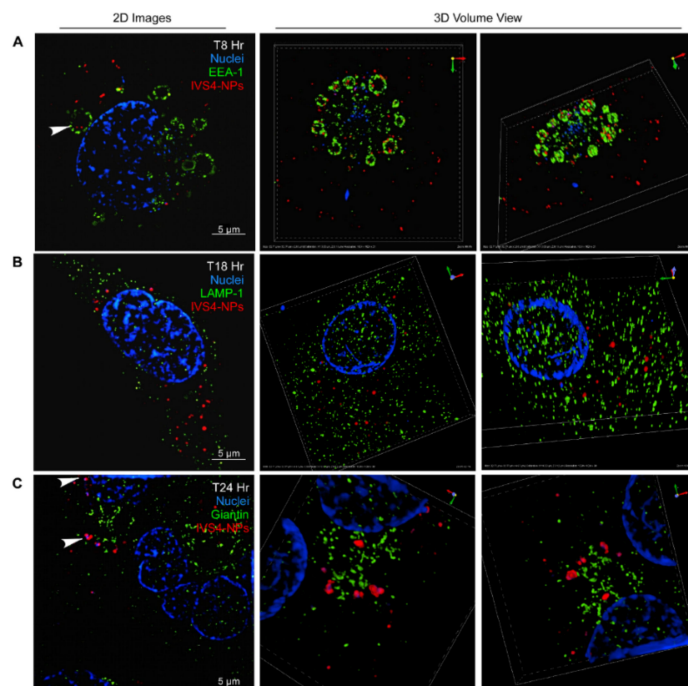


Figure 4. IVS4-Cy3-HGC NPs are endocytosed to the early endosome and then to the Golgi apparatus. (A) The IVS4-Cy3-HGC NPs (red channel) appeared to be entrapped within the spherical structure of the early endosome (green channel) after 8 h of incubation (top panel). (B) While the lysosome (green channel) is typically the next compartment encountered during endocytosis, no co-localization with the NPs was observed at any time point (middle panel). (C) Instead, the NPs appeared to be enmeshed within the structure of the Golgi apparatus (green channel) 24 h post delivery (bottom panel).

Based on the established route of receptor-mediated endocytosis and the data presented by several other groups working with nanoparticles [27–29], we expected the IVS4-Cy3-HGC NPs to co-localize with the lysosomes. However, in our system, no such co-localization was observed at any timepoint over the course of 24 h, as evidenced by the endocytosis assay and subsequent SIM analysis on cells stained for lysosomal-associated membrane protein-1 (LAMP-1) (Figure 4B). It is widely known that in retrograde transport, material can be transferred directly from the early endosome to the Golgi network [30]. Indeed, MMP-14 itself travels along the route as part of the recycling pathway of endocytosis [31,32]. Preliminary SIM analysis of endocytosis assays, in which staining was performed for the Golgi (anti-Giantin), indicated that the NPs co-localized with this structure by 24 h, as evidenced by the presence of 1–2 µm clusters within the lumen of the Golgi (Figure 4C).

3.4. Encapsulation of Cytotoxin Ansamitocin P-3 in IVS4-Cy3-HGC-NPs and System Characterization

After establishing our NP system as selective to MMP-14-expressing cells, capable of inhibiting MMP-14-mediated migration and able to be endocytosed, we then sought

to “weaponize” our system by encapsulating a pharmaceutical agent. The NPs were loaded with the potent microtubule destabilizer ansamitocin P-3 (AP3, Figure 5A), a drug demonstrated to have powerful cytotoxic effects in both preclinical and clinical studies [12,13]. Encapsulation efficiency was measured by UV–vis spectroscopy to be 7.1%, and the loading capacity was calculated to be 0.5%. Although the loading of AP3 was less efficient than the reported values for doxorubicin (DOX)-loaded HGC nanoparticles, we hypothesize that this was due to chemical differences between DOX and AP3 and the steric hindrance caused by the presence of biotin and avidin molecules.

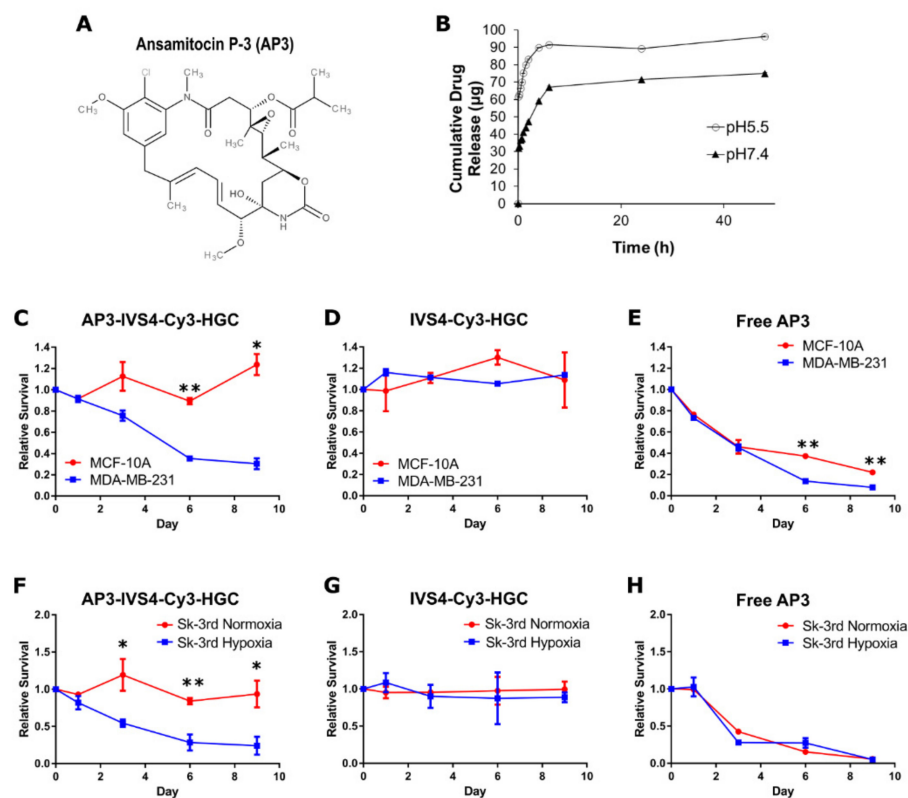


Figure 5. Ansamitocin P3-encapsulated NPs present a pH-dependent release and effectively kill triple-negative breast cancer cells and breast cancer stem cells overexpressing MMP-14 at the membrane. (A) Chemical structure of Ansamitocin P3 (AP3). (B) AP3 was released from AP3-IVS4-HGC NPs in an accelerated manner under acidic conditions (pH 5.5 phosphate buffered saline, PBS), compared to neutral conditions (pH 7.4 PBS). (C) AP3-IVS4-Cy3-HGC NPs efficiently killed only the MMP-14-expressing MDA-MB-231 cancer cells, without affecting the MCF-10A cells. The non-drug-loaded IVS4-Cy3-HGC alone had no effect on viability of either cell type (D), whereas free AP3 killed both non-cancer breast epithelial cells lacking MMP-14 (MCF-10A) and triple-negative breast cancer cells expressing MMP-14 (MDA-MB-231) (E). (F–H) SK-3rd cells were treated with hypoxia, which induced MMP-14 expression at the cell surface, or normoxia in the control. AP3-IVS4-Cy3-HGC NPs induced significant cell death in the hypoxia-treated cells but had no effect on normoxia-treated cells, which had remained in normoxia (F). In contrast, the IVS4-Cy3-HGC NPs had no effect (G), whereas free AP3 killed SK-3rd cells regardless of their treatment (H). AP3-IVS4-Cy3-HGC NPs were prepared at a concentration of 28.70 ng/mL, which contained a net AP3 content of 250 pM, the same as the AP3 concentration used in the free drug experiments. The AP3-IVS4-Cy3-HGC NPs had the same polymeric mass content (mass of NP minus mass of AP3) as the IVS4-Cy3-HGC NPs, which were prepared at a concentration of 28.55 ng/mL. The CellTiter-Glo Viability Assay (Promega) was used as a readout for cytotoxicity. Data are representative of three independent viability experiments. * $p < 0.05$; ** $p < 0.01$.

As AP3 has been found to be cytotoxic in the picomolar range, we hypothesized that even dilute suspensions of AP3-loaded NPs would be sufficient to kill the target cancer cells. A drug-release experiment was performed at normal physiological pH (7.4) and at pH 5.5, which is in the range of acidic pH values of the endocytic compartment. AP3-IVS4-Cy3-HGC NPs suspended in phosphate buffered saline (PBS) (Figure 5B) showed very rapid drug release at early time points (up to 6 h), followed by much slower rates over the next 42 h. (Figure 5B). The rate of release was notably more rapid under acidic conditions compared to neutral conditions, similar to previous findings [33–37].

3.5. AP3-Loaded IVS4-Cy3-HGC NPs Selectively Induce Cell Death in MMP-14-Expressing Cancer Cells

To test our hypothesis that the NPs can selectively deliver AP3 to MMP-14-expressing cancer cells, we examined the viability of MCF-10A and MDA-MB-231 cells treated with different NPs. As shown in Figure 5, cell death was observed only for MMP-14-expressing MDA-MB-231 cells treated with AP3-loaded IVS4-Cy3-HGC NPs, whereas non-MMP-14-expressing MCF-10A cells demonstrated complete survival comparable to the control (Figure 5C). Non-drug-containing IVS4-Cy3-HGC NPs had no effect on cell viability (Figure 5D), whereas free AP3 efficiently induced cell death in both cell lines (Figure 5E), supporting previously published data [14,38,39].

To determine if the IVS4-NP targeting approach is generalized in cancer cells expressing MMP-14, we used the cancer stem-like SK-3rd cell line, in which MMP-14 is expressed but remains in intracellular storage until a stimulus such as hypoxia promotes transport to the cell membrane, where it becomes functional. Previous research established that increased presence of MMP-14 could be observed at the membrane more than a week after the cells returned to a normoxic state [40]. Not only is hypoxia characteristic of most solid tumors, it also drives cancer progression and aggression. Since cancer stem-like cells are highly metastatic, development of therapeutics capable of killing cells that can escape from the primary tumor into circulation and establish secondary lesions is absolutely critical. We, therefore, investigated if AP3-loaded IVS4-Cy3-HGC NPs would be able to target SK-3rd cancer stem-like cells that were exposed to hypoxia (Figure 5). SK-3rd cells were first incubated at 37 °C for 24 h under either normoxic or hypoxic (1% O₂) conditions, and treated with NPs for up to nine days. AP3-IVS4-Cy3-HGC NPs induced cell death only in the hypoxic cells in which MMP-14 would have been transported to the cell surface, killing greater than 75% of the cells after only nine days (Figure 5F). This indicates that our NP system can selectively target cells induced to be highly invasive after exposure to hypoxia. We observed that exposure to free, unencapsulated AP3 resulted in cell death for all SK-3rd cells, regardless of oxygen level (Figure 5H). In contrast, non-drug-loaded IVS4-Cy3-HGC NPs had no effect on cell viability (Figure 5G).

3.6. AP3-Loaded IVS4-Cy3-HGC NPs Prevent MMP-14-Expressing Cancer Cell Invasion In Vivo

To further validate the efficacy of the developed NP drug delivery system against invasive cancer cells in vivo, the chicken chorioallantoic membrane (CAM) assay was performed to assess tumor growth and invasion through the basement membrane of CAM. The CAM has been widely used as an in vivo model of tumor invasion and is a versatile tool for cancer research [41–44]. We selected a metastatic strain of MDA-MB-231 cells, TMD-231-LM2 [45], which were inoculated onto the chorioallantoic membrane of the egg and subsequently treated four times over the course of one week. Each egg was exposed to AP3-loaded IVS4-Cy3-HGC NPs, IVS4-Cy3-HGC NPs, control peptide-Cy3-HGC NPs, or the NP vehicle. Afterwards, the chicken fetuses were sacrificed, and the CAMs were prepared for analysis.

Histological analysis showed that control CAMs, which did not receive the TMD-231-LM2 grafts, demonstrated normal tissue structure (Figure 6A). CAMs that received the grafts but were treated with the control peptide-Cy3-HGC NPs (Figure 6B) were clearly invasive, as the cancer cells formed large tumor masses extending below the upper

CAM. CAMs that received TMD-231-LM2 grafts and were treated with empty, non-drug-loaded IVS4-Cy3-HGC NPs did not penetrate through the upper CAM (Figure 6C), likely due to the inhibition of MMP-14 activity by the IVS4-presenting NPs. Despite the lack of invasion, however, large tumors still formed on top of the CAM. In direct contrast, CAMs that received the TMD-231-LM2 grafts and were treated with AP3-loaded IVS4-Cy3-HGC demonstrated minuscule tumors or no tumors at all (Figure 6D). The overall structure of these CAMs remained intact and appeared similar to that of the control CAMs, demonstrating that the NPs not only killed MMP-14-expressing tumor cells but also blocked their invasive potential.

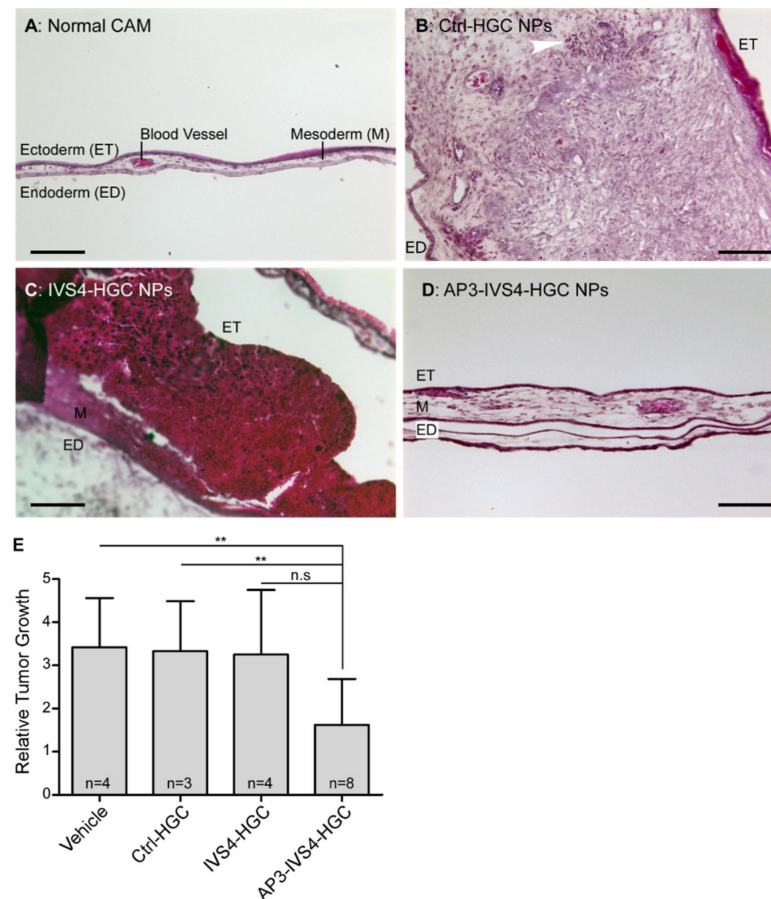


Figure 6. Encapsulation of AP3 by IVS4-Cy3-HGC kills MMP-14-expressing cancer cells and prevents cancer cell invasion in vivo. A total of 10^6 TMD-231 cells were treated as indicated, embedded in a collagen graft (20 μ L total volume), and inoculated on top of the ectoderm layer of the CAM. Treatments (30 μ L) were administered every other day for seven days. Cancer cell invasion into the CAM mesoderm was assessed 7 days post inoculation onto the chick embryos. CAM OCT-embedded sections (8 μ m) were stained with hematoxylin and eosin (H&E). Original magnification \times 200. (A) Normal CAM, which did not receive tumor cells, is presented to demonstrate the normal structure of CAM for comparison. (B) Cells treated with control peptide-Cy3-HGC NPs invaded through the outer membrane of the CAM and developed large tumors. Arrow indicates the invasive edge. (C) TMD-231 grafts treated with IVS4-Cy3-HGC NPs developed large tumors that were minimally invasive and did not break through the outer CAM membrane, instead remaining intact on the CAM surface. (D) No visible tumors are observed in the AP3-IVS4-Cy3-HGC NP-treated CAMs, as the AP3 induced cell death in the MMP-14-expressing cancer cells, while leaving the CAM structure intact. (E) CAMs that received vehicle control, control peptide-Cy3-HGC NPs, or IVS4-Cy3-HGC NPs demonstrated large tumors, whereas treatment with AP3-IVS4-Cy3-HGC NPs significantly prohibited tumor growth. n.s.: not significant, ** $p < 0.01$. All of the treated chickens were viable on the day this experiment ended. Scale bar, 500 μ m.

Of eight CAMs receiving AP3-loaded IVS4-Cy3-HGC NPs, one had a large tumor, two had very small tumors, and the remaining CAMs had no visible tumors. On the other hand, most CAMs in the other treatment groups demonstrated medium or large tumors (Figure 6E). These findings demonstrate that rational design of nanoparticles can lead to selective delivery of a powerful cytotoxin to MMP-14-expressing cancer cells to induce cancer cell death *in vivo* without affecting normal tissue.

4. Discussion

Although the field of nanotherapeutics is rapidly advancing, our understanding of the biological effects of nanomaterials at the molecular and cellular levels remains incomplete. Our previous work clearly demonstrated that a small peptide (IVS4) capable of binding to the hemopexin domain of MMP-14 can block MMP-14 homodimerization, leading to disruption of cell invasion, angiogenesis, and metastasis. Importantly, this work also demonstrated that peptides shown to be selective for the hemopexin domain of MMP-14 have no effect on the functions of MMP-9 or MMP-25 [2]. Since peptides alone are degraded rapidly *in vivo*, we bioconjugated the IVS4 peptide to hydrophobically modified glycol chitosan nanoparticles (NPs). Our strategy was to utilize the inhibitory effect of the IVS4 peptide on MMP-14-functions and confer the NPs with the ability to selectively bind to cancer cells. Moreover, endocytic uptake of the NPs would be enhanced, leading to the release of encapsulated pharmaceutical agents into the cytosol. We also effectively demonstrated, both *in vitro* and *in vivo*, that ansamitocin P-3 (AP3) encapsulated IVS4-NPs were capable of selectively killing MMP-14-expressing cancer cells, without affecting the viability of cells lacking MMP-14 expression at the cell surface (Figure 7). Although AP3 is not an FDA-approved drug, it can serve as a prototypical drug-encapsulation model system that may be used to enhance our understanding of MMP-14-mediated cancer cell fate.

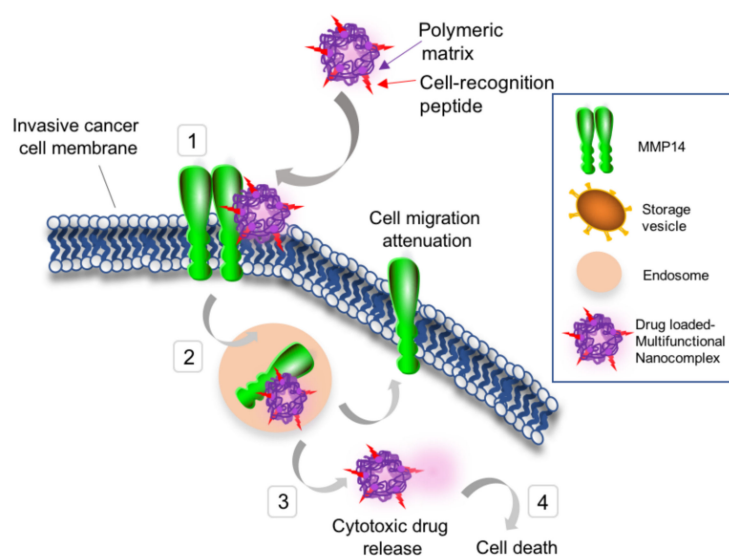


Figure 7. Proposed mechanism of action of the peptide-homing nanoparticles interacting with a cancer cell expressing MMP-14 at its surface. (1) NPs interact with the MMP14, via PEX domain, over-expressed at the membrane of invasive cancer cells; (2) NPs are internalized and routed to endosomes and intracellular vesicles; (3) NPs escape endosomal entrapment and encapsulated cytotoxic drug is released into the cytosol, which can lead to effective cell death (4).

Our present report demonstrates that the bifunctional approach described in this study is capable of attenuating MMP-14-mediated cancer cell functions, including tumor cell invasion, as well as selectively delivering the powerful cytotoxin AP3, a stable microtubule destabilizer that has been tested clinically in cancer patients. We note that severe side effects involving neuronal and gastrointestinal toxicity have been previously observed for AP3 due to off-target effects [14]. Moreover, AP3 is remarkably more cytotoxic against cancer

stem-like cells than Taxol, a chemotherapeutic that has been widely used clinically in breast cancer therapy (unpublished results). As the IVS4-NPs are demonstrated to accumulate prominently in MMP-14-expressing cancer cells, this drug delivery system is expected to specifically target tumors, thereby bypassing off-target tissues. The high potency of AP3, combined with the long-term steady release observed from the NP system, could possibly lead to lower dosages necessary for administration in vivo.

It has been widely accepted that the acidic pH of endosomes causes nanoparticles to disassemble at an accelerated rate and release encapsulated drugs more rapidly [46]. We observed that the overall structure of endosomes changes significantly over time after the NPs are endocytosed and attribute these changes to the proton sponge effect [47], which suggests that cationic polymers buffer the acidic pH of the endosome, leading to an influx of counterions that cause the endosome to swell and rupture. As AP3 is a potent microtubule destabilizer, its release from the NP into the cytoplasm is a requisite for pharmacological activity. The proton sponge effect provides a plausible mechanism, by which AP3 is released and is able to remain active.

Our previous work using a chicken chorioallantoic membrane (CAM) angiogenesis model [2] demonstrated that the MMP-14-selective IVS4 peptide can attenuate new blood vessel growth. As angiogenesis inhibitors are often co-administered with chemotherapeutics, we propose that AP3-loaded IVS4-NPs could also minimize angiogenesis. Collectively, the IVS4-functionalized NP system may potentially target angiogenesis, cancer cell invasion, and metastasis and simultaneously deliver a cytotoxin to metastatic cancer cells. These promising preliminary results suggest that our nanotherapeutic has much clinical potential as a target-specific anticancer therapy.

5. Conclusions

In this study, cancer-homing micellar nanoparticles (NPs) were assembled by linking the IVS4 peptide to hydrophobically modified glycol chitosan (HGC) via an avidin–biotin binding strategy. The NPs were preferentially taken up by MMP-14-expressing cells and prevented MMP-14-mediated cell migration. Encapsulation of the cytotoxin ansamitocin P-3 induced cell death in MDA-MB-231 breast cancer cells and Sk-3rd breast cancer stem cells, whereas the non-drug-loaded IVS4-NPs were found to be noncytotoxic. Additionally, IVS4-NPs attenuated cancer cell invasion and killed MMP-14-expressing tumor cells in a chicken chorioallantoic membrane assay. Our results demonstrated that drug-loaded IVS4-HGC NPs can specifically target MMP14-expressing cells and have the potential to be used as a novel nanotherapeutic for treating metastatic cancer.

Supplementary Materials: The following supporting information can be downloaded at: <https://www.mdpi.com/article/10.3390/biophysica2030021/s1>, Figure S1: Cell viability of cancerous and non-cancerous breast cancer cells treated with empty NP vehicles; Figure S2: Schematic of the experimental protocol for the in vitro endocytosis assay; Figure S3: Super-resolution structured illumination microscopy images of MDA-MB-231 cells.

Author Contributions: J.C. (Jian Cao) and Y.M. conceived and supervised the project. J.C. (Jillian Cathcart) performed and analyzed all protein purification, cell biology, and chicken chorioallantoic membrane experiments, with the help of G.S. and W.L. G.S. and W.L. synthesized and characterized the nanoparticles. J.C. (Jillian Cathcart), G.S., J.C. (Jian Cao), and Y.M. wrote the manuscript. All authors have read and agreed to the published version of the manuscript.

Funding: This work was supported by a grant from the National Institutes of Health (1R01CA166936-03).

Informed Consent Statement: Not applicable.

Data Availability Statement: Not applicable.

Acknowledgments: We would like to acknowledge Markus Seeliger and Ivan Lebedev of Stony Brook University (Department of Pharmacology and Biochemistry and Department of Structural Biology, respectively) for their effort and time assisting with the purification and subsequent validation of the PEX protein. We would also like to acknowledge Jingxuan Liu of Stony Brook University's Department of Pathology for their time and assistance in the analysis of the CAM experiment results.

Conflicts of Interest: The authors declare no conflict of interest.

Abbreviations

ADAM	a disintegrin and metalloproteinase
AP3	ansamitocin P-3
CAM	chorioallantoic membrane
DLS	dynamic light scattering
DMEM	Dulbecco's Modified Eagle Medium
DMSO	dimethylsulfoxide
DOX	doxorubicin
EDC	N-(3-dimethylaminopropyl)-N'-ethylcarbodiimide hydrochloride
EEA-1	early endosome antigen-1
ECM	extracellular matrix
GC	glycol chitosan
HGC	hydrophobically modified glycol chitosan
HPLC	High-performance liquid chromatography
HRP	Horseradish peroxidase
LAMP-1	lysosomal-associated membrane protein-1
MMP-14	matrix metalloproteinase-14
MMPI	matrix metalloproteinase inhibitor
MT1-MMP	membrane type 1 matrix metalloproteinase
MWCO	molecular weight cut-off
NHS	N-hydroxysuccinimide
NP	nanoparticle
PBS	Phosphate-buffered saline
PCR	polymerase chain reaction
PEX	hemopexin
SDS-PAGE	sodium dodecyl sulfate–polyacrylamide gel electrophoresis
SIM	structure illumination microscopy
TEM	transmission electron microscopy

References

- Hanahan, D.; Weinberg, R.A. Hallmarks of Cancer: The Next Generation. *Cell* **2011**, *144*, 646–674. [[CrossRef](#)] [[PubMed](#)]
- Zarrabi, K.; Dufour, A.; Li, J.; Kuscu, C.; Pulkoski-Gross, A.; Zhi, J.; Hu, Y.; Sampson, N.S.; Zucker, S.; Cao, J. Inhibition of Matrix Metalloproteinase 14 (MMP-14)-mediated Cancer Cell Migration. *J. Biol. Chem.* **2011**, *286*, 33167–33177. [[CrossRef](#)] [[PubMed](#)]
- Cao, J.; Chiarelli, C.; Kozarekar, P.; Adler, H.L. Membrane type 1-matrix metalloproteinase promotes human prostate cancer invasion and metastasis. *Thromb. Haemost.* **2005**, *93*, 770–778. [[PubMed](#)]
- Itoh, T.; Tanioka, M.; Yoshida, H.; Yoshioka, T.; Nishimoto, H.; Itohara, S. Reduced angiogenesis and tumor progression in gelatinase A-deficient mice. *Cancer Res.* **1998**, *58*, 1048–1051. [[PubMed](#)]
- Chun, T.-H.; Sabeh, F.; Ota, I.; Murphy, H.; McDonagh, K.T.; Holmbeck, K.; Birkedal-Hansen, H.; Allen, E.D.; Weiss, S.J. MT1-MMP-dependent neovessel formation within the confines of the three-dimensional extracellular matrix. *J. Cell Biol.* **2004**, *167*, 757–767. [[CrossRef](#)]
- Tsunezuka, Y.; Kinoh, H.; Takino, T.; Watanabe, Y.; Okada, Y.; Shinagawa, A.; Sato, H.; Seiki, M. Expression of membrane-type matrix metalloproteinase 1 (MT1-MMP) in tumor cells enhances pulmonary metastasis in an experimental metastasis assay. *Cancer Res.* **1996**, *56*, 5678–5683. [[PubMed](#)]
- Yonemura, Y.; Endo, Y.; Takino, T.; Sakamoto, K.; Bandou, E.; Kinoshita, K.; Fushida, S.; Miwa, K.; Sugiyama, K.; Sasaki, T. Membrane-type 1 matrix metalloproteinase enhances lymph node metastasis of gastric cancer. *Clin. Exp. Metastasis* **2000**, *18*, 321–327. [[CrossRef](#)]
- Egeblad, M.; Werb, Z. New functions for the matrix metalloproteinases in cancer progression. *Nat. Rev. Cancer* **2002**, *2*, 161–174. [[CrossRef](#)]
- Massova, I.; Kotra, L.P.; Fridman, R.; Mobashery, S. Matrix metalloproteinases: Structures, evolution, and diversification. *FASEB J.* **1998**, *12*, 1075–1095. [[CrossRef](#)]

10. Matthews, B.W. Structural basis of the action of thermolysin and related zinc peptidases. *Acc. Chem. Res.* **1988**, *21*, 333–340. [[CrossRef](#)]
11. Nagase, H.; Visse, R.; Murphy, G. Structure and function of matrix metalloproteinases and TIMPs. *Cardiovasc. Res.* **2006**, *69*, 562–573. [[CrossRef](#)]
12. Tassone, P.; Gozzini, A.; Goldmacher, V.; Shammas, M.A.; Whiteman, K.R.; Carrasco, D.R.; Li, C.; Allam, C.K.; Venuta, S.; Anderson, K.C. In vitro and in vivo activity of the maytansinoid immunoconjugate huN901-N2'-deacetyl-N2'-(3-mercapto-1-oxopropyl)-maytansine against CD56+ multiple myeloma cells. *Cancer Res.* **2004**, *64*, 4629–4636. [[CrossRef](#)]
13. Ikeda, H.; Hideshima, T.; Fulciniti, M.; Lutz, R.J.; Yasui, H.; Okawa, Y.; Kiziltepe, T.; Vallet, S.; Pozzi, S.; Santo, L. The monoclonal antibody nBT062 conjugated to cytotoxic Maytansinoids has selective cytotoxicity against CD138-positive multiple myeloma cells in vitro and in vivo. *Clin. Cancer Res.* **2009**, *15*, 4028–4037. [[CrossRef](#)]
14. Venghateri, J.B.; Gupta, T.K.; Verma, P.J.; Kunwar, A.; Panda, D. Ansamitocin P3 depolymerizes microtubules and induces apoptosis by binding to tubulin at the vinblastine site. *PLoS ONE* **2013**, *8*, e75182.
15. Ericsson, U.B.; Hallberg, B.M.; DeTitta, G.T.; Dekker, N.; Nordlund, P. Thermofluor-based high-throughput stability optimization of proteins for structural studies. *Anal. Biochem.* **2006**, *357*, 289–298. [[CrossRef](#)]
16. Cho, K.; Wang, X.; Nie, S.; Shin, D.M. Therapeutic nanoparticles for drug delivery in cancer. *Clin. Cancer Res.* **2008**, *14*, 1310–1316. [[CrossRef](#)]
17. Cao, J.; Hymowitz, M.; Conner, C.; Bahou, W.F.; Zucker, S. The propeptide domain of membrane type 1-matrix metalloproteinase acts as an intramolecular chaperone when expressed in trans with the mature sequence in COS-1 cells. *J. Biol. Chem.* **2000**, *275*, 29648–29653. [[CrossRef](#)]
18. Evensen, N.A.; Li, J.; Yang, J.; Yu, X.; Sampson, N.S.; Zucker, S.; Cao, J. Development of a high-throughput three-dimensional invasion assay for anti-cancer drug discovery. *PLoS ONE* **2013**, *8*, e8281. [[CrossRef](#)]
19. Lokman, N.A.; Elder, A.S.; Ricciardelli, C.; Oehler, M.K. Chick chorioallantoic membrane (CAM) assay as an in vivo model to study the effect of newly identified molecules on ovarian cancer invasion and metastasis. *Int. J. Mol. Sci.* **2012**, *13*, 9959–9970. [[CrossRef](#)]
20. Suarato, G.; Lee, S.I.; Li, W.; Rao, S.; Khan, T.; Meng, Y.; Shelly, M. Micellar nanocomplexes for biomagnetic delivery of intracellular proteins to dictate axon formation during neuronal development. *Biomaterials* **2017**, *112*, 176–191. [[CrossRef](#)]
21. Yin, W.; Li, W.; Rubenstein, D.A.; Meng, Y. Biocompatible and target specific hydrophobically modified glycol chitosan nanoparticles. *Biointerphases* **2016**, *11*, 04B301. [[CrossRef](#)]
22. Jayakumar, R.; Chennazhi, K.P.; Muzzarelli, R.A.A.; Tamura, H.; Nair, S.V.; Selvamurugan, N. Chitosan conjugated DNA nanoparticles in gene therapy. *Carbohydr. Polym.* **2010**, *79*, 1–8. [[CrossRef](#)]
23. Park, K.; Kim, J.-H.; Nam, Y.S.; Lee, S.; Nam, H.Y.; Kim, K.; Park, J.H.; Kim, I.-S.; Choi, K.; Kim, S.Y. Effect of polymer molecular weight on the tumor targeting characteristics of self-assembled glycol chitosan nanoparticles. *J. Control. Release* **2007**, *122*, 305–314. [[CrossRef](#)]
24. Chin, A.; Suarato, G.; Meng, Y. Evaluation of physicochemical characteristics of hydrophobically modified glycol chitosan nano-particles and their biocompatibility in murine osteosarcoma and osteoblast-like cells. *J. Nanotech. Smart Mater.* **2014**, *1*, 1–7.
25. Duceppe, N.; Tabrizian, M. Advances in using chitosan-based nanoparticles for in vitro and in vivo drug and gene delivery. *Expert Opin. Drug Deliv.* **2010**, *7*, 1191–1207. [[CrossRef](#)]
26. Bacac, M.; Fusco, C.; Planche, A.; Santodomingo, J.; Demareux, N.; Leemann-Zakaryan, R.; Provero, P.; Stamenkovic, I. Securin and separate modulate membrane traffic by affecting endosomal acidification. *Traffic* **2011**, *12*, 615–626. [[CrossRef](#)]
27. Salvati, A.; Åberg, C.; dos Santos, T.; Varela, J.; Pinto, P.; Lynch, I.; Dawson, K.A. Experimental and theoretical comparison of intracellular import of polymeric nanoparticles and small molecules: Toward models of uptake kinetics. *Nanomed. Nanotechnol. Biol. Med.* **2011**, *7*, 818–826. [[CrossRef](#)]
28. Nam, H.Y.; Kwon, S.M.; Chung, H.; Lee, S.-Y.; Kwon, S.-H.; Jeon, H.; Kim, Y.; Park, J.H.; Kim, J.; Her, S. Cellular uptake mechanism and intracellular fate of hydrophobically modified glycol chitosan nanoparticles. *J. Control. Release* **2009**, *135*, 259–267. [[CrossRef](#)]
29. Park, S.; Lee, S.J.; Chung, H.; Her, S.; Choi, Y.; Kim, K.; Choi, K.; Kwon, I.C. Cellular uptake pathway and drug release characteristics of drug-encapsulated glycol chitosan nanoparticles in live cells. *Microsc. Res. Tech.* **2010**, *73*, 857–865. [[CrossRef](#)]
30. Bonifacino, J.S.; Rojas, R. Retrograde transport from endosomes to the trans-Golgi network. *Nat. Rev. Mol. Cell Biol.* **2006**, *7*, 568–579. [[CrossRef](#)]
31. Wang, X.; Ma, D.; Keski-Oja, J.; Pei, D. Co-recycling of MT1-MMP and MT3-MMP through the Trans-Golgi Network: Identification of DKV582 as a recycling signal. *J. Biol. Chem.* **2004**, *279*, 9331–9336. [[CrossRef](#)] [[PubMed](#)]
32. Rémacle, A.; Murphy, G.; Roghi, C. Membrane type I-matrix metalloproteinase (MT1-MMP) is internalised by two different pathways and is recycled to the cell surface. *J. Cell Sci.* **2003**, *116*, 3905–3916. [[CrossRef](#)] [[PubMed](#)]
33. Zhao, Y.; Guo, Y.; Li, R.; Wang, T.; Han, M.; Zhu, C.; Wang, X. Methotrexate Nanoparticles Prepared with Codendrimer from Polyamidoamine (PAMAM) and Oligoethylene Glycols (OEG) Dendrons: Antitumor Efficacy In Vitro and In Vivo. *Sci. Rep.* **2016**, *6*, 28983. [[CrossRef](#)] [[PubMed](#)]
34. Hrubý, M.; Koňák, Č.; Ulbrich, K. Polymeric micellar pH-sensitive drug delivery system for doxorubicin. *J. Control. Release* **2005**, *103*, 137–148. [[CrossRef](#)]
35. Missirlis, D.; Kawamura, R.; Tirelli, N.; Hubbell, J.A. Doxorubicin encapsulation and diffusional release from stable, polymeric, hydrogel nanoparticles. *Eur. J. Pharm. Sci.* **2006**, *29*, 120–129. [[CrossRef](#)]

36. Wang, J.J.; Zeng, Z.W.; Xiao, R.Z.; Xie, T.; Zhou, G.L.; Zhan, X.R.; Wang, S.L. Recent advances of chitosan nanoparticles as drug carriers. *Int. J. Nanomed.* **2011**, *6*, 765–774.
37. Min, K.H.; Park, K.; Kim, Y.-S.; Bae, S.M.; Lee, S.; Jo, H.G.; Park, R.-W.; Kim, I.-S.; Jeong, S.Y.; Kim, K.; et al. Hydrophobically modified glycol chitosan nanoparticles-encapsulated camptothecin enhance the drug stability and tumor targeting in cancer therapy. *J. Control. Release* **2008**, *127*, 208–218. [[CrossRef](#)]
38. Wolpert-Defilippes, M.; Adamson, R.; Cysyk, R.; Johns, D. Initial studies on the cytotoxic action of maytansine, a novel ansa macrolide. *Biochem. Pharmacol.* **1975**, *24*, 751–754. [[CrossRef](#)]
39. Kupchan, S.M.; Komoda, Y.; Court, W.; Thomas, G.; Smith, R.; Karim, A.; Gilmore, C.; Haltiwanger, R.; Bryan, R. Tumor inhibitors. LXXIII. Maytansine, a novel antileukemic ansa macrolide from *Maytenus ovatus*. *J. Am. Chem. Soc.* **1972**, *94*, 1354–1356. [[CrossRef](#)]
40. Li, J.; Zucker, S.; Pulkoski-Gross, A.; Kuscu, C.; Karaayvaz, M.; Ju, J.; Yao, H.; Song, E.; Cao, J. Conversion of stationary to invasive tumor initiating cells (TICs): Role of hypoxia in membrane type 1-matrix metalloproteinase (MT1-MMP) trafficking. *PLoS ONE* **2012**, *7*, e38403. [[CrossRef](#)]
41. Nowak-Sliwinska, P.; Segura, T.; Iruela-Arispe, M.L. The chicken chorioallantoic membrane model in biology, medicine and bioengineering. *Angiogenesis* **2014**, *17*, 779–804. [[CrossRef](#)]
42. Sabeih, F.; Ota, I.; Holmbeck, K.; Birkedal-Hansen, H.; Soloway, P.; Balbin, M.; Lopez-Otin, C.; Shapiro, S.; Inada, M.; Krane, S.; et al. Tumor cell traffic through the extracellular matrix is controlled by the membrane-anchored collagenase MT1-MMP. *J. Cell Biol.* **2004**, *167*, 769–781. [[CrossRef](#)]
43. Liu, M.; Scanlon, C.S.; Banerjee, R.; Russo, N.; Inglehart, R.C.; Willis, A.L.; Weiss, S.J.; D’Silva, N.J. The Histone Methyltransferase EZH2 Mediates Tumor Progression on the Chick Chorioallantoic Membrane Assay, a Novel Model of Head and Neck Squamous Cell Carcinoma. *Transl. Oncol.* **2013**, *6*, 273–281. [[CrossRef](#)]
44. Rowe, R.G.; Li, X.Y.; Hu, Y.; Saunders, T.L.; Virtanen, I.; de Herreros, A.G.; Becker, K.F.; Ingvarsen, S.; Engelholm, L.H.; Bommer, G.T.; et al. Mesenchymal cells reactivate Snail1 expression to drive three-dimensional invasion programs. *J. Cell Biol.* **2009**, *184*, 399–408. [[CrossRef](#)]
45. Helbig, G.; Christopherson, K.W.; Bhat-Nakshatri, P.; Kumar, S.; Kishimoto, H.; Miller, K.D.; Broxmeyer, H.E.; Nakshatri, H. NF- κ B promotes breast cancer cell migration and metastasis by inducing the expression of the chemokine receptor CXCR4. *J. Biol. Chem.* **2003**, *278*, 21631–21638. [[CrossRef](#)]
46. Suarato, G.; Li, W.; Meng, Y. Role of pH-responsiveness in the design of chitosan-based cancer nanotherapeutics: A review. *Biointerphases* **2016**, *11*, 04B201. [[CrossRef](#)]
47. Li, W.Y.; Suarato, G.; Cathcart, J.M.; Sargunas, P.R.; Meng, Y.Z. Design, characterization, and intracellular trafficking of biofunctionalized chitosan nanomicelles. *Biointerphases* **2020**, *15*, 14. [[CrossRef](#)]